To appear in *Vehicle System Dynamics*
Vol. 00, No. 00, Month 20XX, 1–17

An Experimental Investigation of the Bicycle Motion during a Hands-On Shimmy

Nicolò Tomiati, Gianantonio Magnani, and Marco Marcon*

Dipartimento di Elettronica, Informazione e Bioingegneria (DEIB),
Politecnico di Milano, via Ponzio 34/5, 20133, Milan, Italy

(*Received 00 Month 20XX; accepted 00 Month 20XX*)

This paper presents original data records of linear accelerations and angular velocities of six points of a racing bicycle collected during a "genuine" hands-on shimmy. The records, together with GPS, forward speed data, and action cam videos are thoroughly analysed to understand the actual motion of the bicycle and its parts, at lower (weave) and higher (wobble or shimmy) frequencies. The main goal is to assess how and to what extent each part, and what compliances, are involved in the shimmy mechanism. In particular, the motions of the front and rear frames, and thus of the whole bicycle, during shimmy are carefully rebuilt. At higher frequencies, the bicycle frame rotates rigidly about an axis parallel to the yaw axis, while it undergoes a relative torsion between the head tube and the dropouts in the longitudinal (roll) direction. Likewise, the front frame rotates rigidly about the steering axis (in the entire frequency range), while it bends laterally consistently with the bicycle frame torsion. Although the overall motion is very complex, these results validate and extend models, conjectures, and theoretical results of the scientific literature about shimmy.

Keywords: shimmy; wobble; bicycle; vibrations; data acquisition system; inertial measurement unit

1. Introduction

Shimmy, also known as *wobble* or *speed wobble*, is one of the most frightening and dangerous dynamic instabilities that may occur while riding a bicycle or a motorcycle. Shimmy can be described as an oscillation of the bicycle steering assembly at frequencies too high (6-10 Hz) for an effective reaction of the rider. A good idea of the behaviour of a bicycle subjected to shimmy can be found, for example, in [1–5]. Shimmy may occur *hands-off*, possibly intentionally induced by the rider as in [5], but it is especially scaring when it suddenly onsets while riding high-speed with the hands firmly holding the handlebar (*hands-on* shimmy), as the rider feels the bicycle out of control and can only try not to fall and reduce the speed by braking carefully, at first, as braking may increase the amplitude of the oscillations. No specific factors related to the wobble onset have been identified up to now, except for high speed (generally over 14 m/s in racing bicycles). Among those mentioned in popular literature, we share tremors and stiffness of the rider arms, e.g. due to cold weather, and the particularly wrinkled asphalt. Shimmy is well known to bicycle manufacturers, to expert, and to both professional riders and amateurs [6], even if it is rarely mentioned despite its dangerousness for the safety of riders.

*Corresponding author. Email: marco.marcon@polimi.it

The rigid-body analysis of bicycle oscillations predicts oscillations of frequencies much lower than that of shimmy [7], and it is agreed that to predict shimmy it is necessary to introduce additional (elastic) degrees of freedom. These can be found in the front and rear frames compliances, which define certain structural bicycle properties, and in the elasticity and dynamics of the tires. To some extent also the rider, his hands, arms, body structure, and his driving style can help to create favourable conditions for the shimmy onset [8–13].

Most of the literature results are model-based and supported by laboratory tests, while little "genuine" on-road measurement data are available to validate the numerical models. The first contribution of this paper is to provide unique data records of linear accelerations and angular velocities of six points of a professional racing bicycle collected together with GPS, forward speed data, and action cam videos during a true high-speed hands-on shimmy. The *ad hoc* data acquisition system consists of a central single board computer (Raspberry Pi) driving six microcontrollers (Arduino boards) equipped with Inertial Measurement Units (IMU), each able to measure the three components of the linear acceleration and of the angular velocity. Measurements are sampled every 0.005 s (f_s = 200 Hz), and the sampling is controlled by the central unit with a single digital output (DO) signal to ensure the synchronous sample of all IMU measures.

Then, the records are thoroughly analysed to investigate the actual motion of the bicycle and its parts at lower (weave) and higher (wobble or shimmy) frequencies, with the purpose of assessing how and to what extent each part is involved in the shimmy mechanism, and where the relevant compliances are located. In particular, the motions of the front (front wheel, fork, head tube, stem, and handlebar) and rear (bicycle frame and rear wheel) frames, and thus of the whole bicycle, are carefully rebuilt at the wobble frequency of about 7 Hz. At this frequency, the bicycle frame rotates rigidly about an axis parallel to the yaw axis, while it undergoes a relative torsion between the head tube and the dropouts in the longitudinal (roll) direction. Likewise, the front frame rotates rigidly about the steering axis (in the whole frequency range) while it bends laterally consistently with the bicycle frame torsion. These results validate and extend models, conjectures, and theoretical results of the scientific literature about shimmy. In addition, they help to devise changes to bicycle design to make shimmy-free (better, less prone to shimmy) bicycles.

The paper is organised as follow. In Section 2, the data acquisition system is presented. In Section 3, the bicycle setup and the on-road test activity are described. Then, in Section 4, the linear acceleration and angular velocity records are presented and analysed, and the resulting motions and compliances of the front and rear frames as well as of the whole bicycle are commented. Finally, Section 5 analyzes the main results and in Section 6 conclusions are drawn.

2. Data Acquisition System Architecture

The Data Acquisition System (DAS) architecture represented in Figure 1 is based on a Central Unit (CU) formed by an Embedded PC: a Raspberry Pi II [14], and on six Inertial Measurement Units (IMUx, where x is the board number) each integrated into an Arduino (Genuino) 101 device [15]. Each Arduino 101 is connected to the CU by a USB cable through a USB hub (since the Raspberry Pi has only four USB ports). The Raspberry Pi and the USB hub are powered using a power bank of 20 Ah placed on the bicycle seat tube while the Arduino 101 boards are directly powered from the USB cable.

Every Arduino 101 is equipped with a Dual Core Intel® Curie™ system module [16]

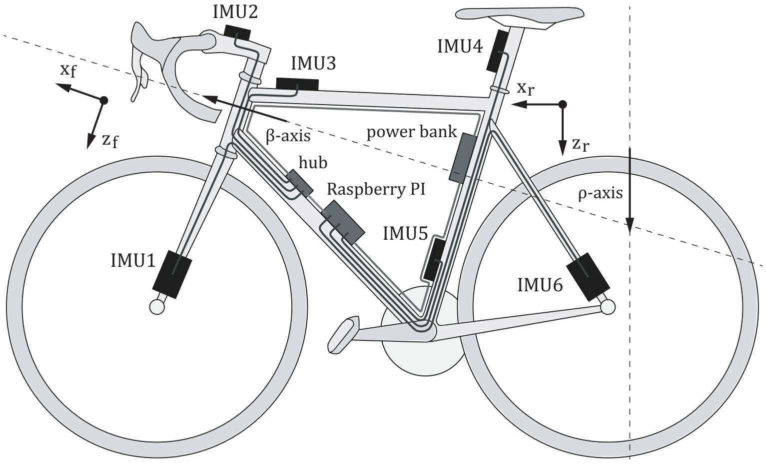

Figure 1. Data Acquisition System (DAS) installed on the racing bicycle with left-handed reference systems for the front and rear frames.

working at 32 MHz clock; inside the Intel Curie Module there is a Bosch BMI160 6-axis Sensing Device built with an accelerometer and a gyroscope, both with 16 bit resolution. The Bosch sensor [17] was set at a reading time of 200 samples per second and the acquisition range was set to $\pm 16\ g$ for the accelerometer and $\pm 250\ ^{\circ}/s$ for the gyroscope.

For our acquisition system the synchronization between the six IMUs is crucial in order to analyse the simultaneous bicycle motion and deformation. Due to the latency of the USB 2.0 port, to the random delay introduced from the software querying sequence on each IMU, and to the further delay introduced by the USB hub, implementing a hardware synchronization was mandatory. In particular, we used one DIO (Digital Input/Output) pin of the Raspberry Pi GPIO (General Purpose Input Output) as a synchronization signal for all the IMUs. We controlled it using the WiringPi library [18] and, generating a square wave on this output pin, it becomes a pacer for all the IMUs: every Arduino 101 waits for this signal in order to read the accelerometer and the gyroscope measures and then send the sampled data to the USB serial connection. Even if the data acquired synchronously from different IMUs reach the CU with a variable delay (due to the USB bus) we can ensure that all the samples are synchronized with the pacer signal. Every Arduino 101 sends then a packet with the data and a univocal header that are stored in a single file; the timestamp associated to each packet is the global time of the Raspberry Pi board when the pacer impulse is issued. All data are stored in a binary form and are then processed offline with a MATLAB® [19] script.

In order to make the whole system compact and stand-alone without requiring any external control device, we integrated a start and stop button, and a LED on the GPIO connector of the CU. This allows us to easily enable and disable data acquisition, verifying the proper recording of the acquired data through the blinking LED.

3. On-road Experimental Activity

In this Section the setup of the on-road experimental activity is discussed. The bicycle under test is a professional carbon-fiber racing bike, size 52S, with professional equipment. Data regarding its geometric, mass, stiffness, and damping properties can be found in [20]. The DAS is installed on the bicycle, as shown in Figure 1. In particular:

- two IMUs are fastened on the front frame of the bicycle: IMU1 near the front

Figure 2. Rider's posture during the on-road test.

wheel hub and IMU2 on the stem;
- four IMUs are fixed on the rear frame: IMU3 on the horizontal top tube near the head tube, IMU4 on the seat post under the saddle, IMU5 on the seat tube near the bottom bracket, and IMU6 near the rear wheel hub;
- the power bank unit is installed on the seat tube between IMU4 and IMU5. It supplies current to both the Raspberry Pi and the USB hub;
- the Raspberry Pi is fastened on the down tube of the bicycle frame near the bottom bracket. It is connected to the power bank through the micro USB socket, while USB 2.0 connectors and jumpers are used to link the Raspberry Pi to the USB hub and to IMU4, IMU5, and IMU6;
- the USB hub is installed near the Raspberry Pi and it is connected to the power bank, to the Raspberry Pi, and to IMU1, IMU2, and IMU3;
- the Garmin Edge 820® [21] sensor unit is installed on the front wheel hub, while the computer touch screen is located on the handlebar near IMU2;
- two GoPro HERO3+® [22] are used in the video mode with a resolution of 960 pixel and 100 frames per second. One of them is fixed under the saddle, pointing the rear wheel and its hub. The other one is located on the rider's chest, pointing in the forward direction and trying to capture the motion of the bicycle front assembly.

The Garmin Edge 820 can collect and store different measured data: distance, speed, altitude, latitude, longitude, and temperature. From distance travelled and altitude data, information on the road slope can be easily derived.

During the on-road tests, the rider was followed by a car equipped with a video camera on its roof. In doing so, it was possible to see the bicycle and the rider body moving from a point of view external to the bicycle.

Figure 2 shows the rider's posture during the on-road test. His upper torso is bent forward to assume an aerodynamic configuration and his hands firmly tighten the handlebar.

3.1. *Test Campaign*

In November 2017 a test day was organized near Lecco (Lombardy, Italy), at the Bevera downhill. Figure 3 shows the path of the on-road test.

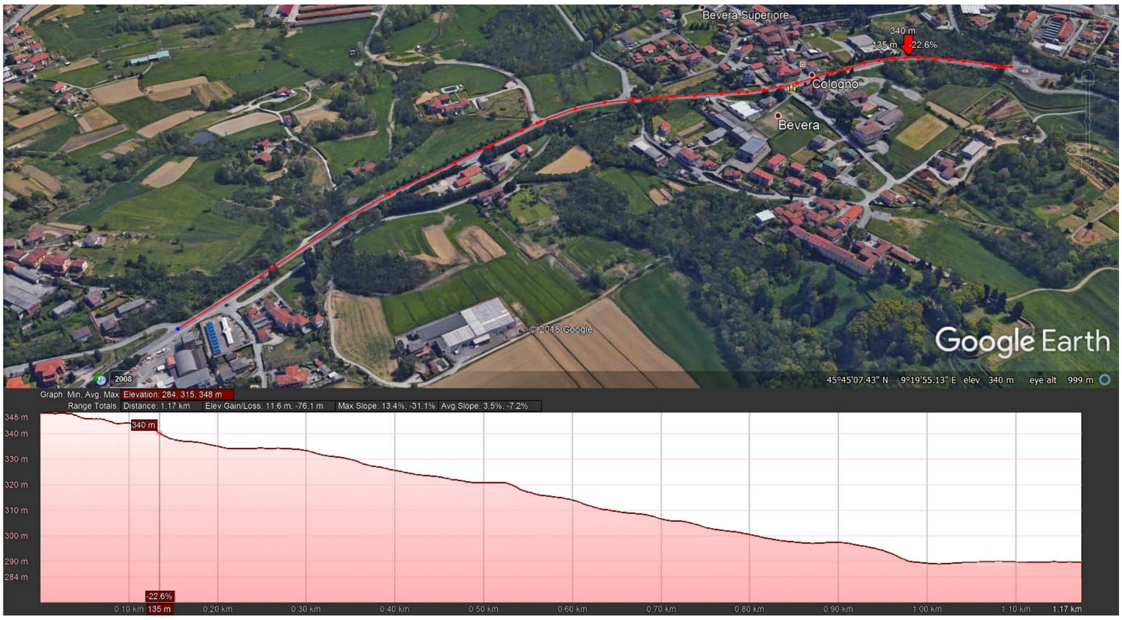

Figure 3. The place and the path of the on-road test at the Bevera downhill (Lecco, Lombardy, Italy).

Table 1. Tyres and rims characteristics.

Tyre set	ETRTO size	Rim inner width	Inflation pressure
A	22-622	15c	7 bar
B	25-622	15c	7 bar

Two different sets of tyres were tested to check the influence on shimmy occurrence (Table 1 summarizes their characteristics). Same inflation pressure was used for both front and rear wheel. The experimental activity basically consists of riding downhill trying to reach a speed in the range 14–18 m/s towards the end of the descent, where the road slope starts to decrease. This choice is based on safety reasons: while brakes can be used only to a small extent during shimmy, the road becoming flat ensures the speed reduction needed to damp out wobble. The same descent was repeated three times for the two different tyres and, during each test, no disturbances or external triggers were applied to promote the shimmy onset.

4. Test Results

All tests were performed hands-on, namely, the rider's hands were firmly tightened on the handlebar during the descents. Shimmy appeared in two tests out of six, with the same tyres (model A) mounted on the bicycle. In one of them, a quite large oscillation occurred, although not so violent as the shimmies experienced by Gianantonio Magnani in 2011 and 2014, as described in [23] and [8]. During the wobble occurrence, the cyclist was not pedalling.

Figure 4 shows the time plots of the lateral acceleration, roll and yaw angular velocities recorded by IMU2 on the stem during shimmy. All signals are filtered with a low-pass filter with a cut-off frequency $f_c = 20$ Hz to remove high-frequency noise. As can be seen in the lateral acceleration plot, there are three sudden jumps in wobble amplitude. They are probably due to a slight change in the rider's upper body position as confirmed

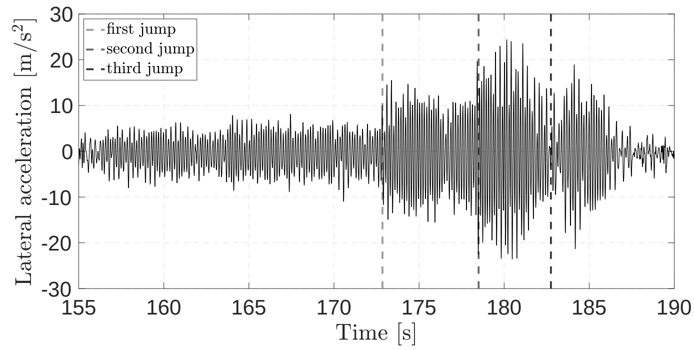

(a)

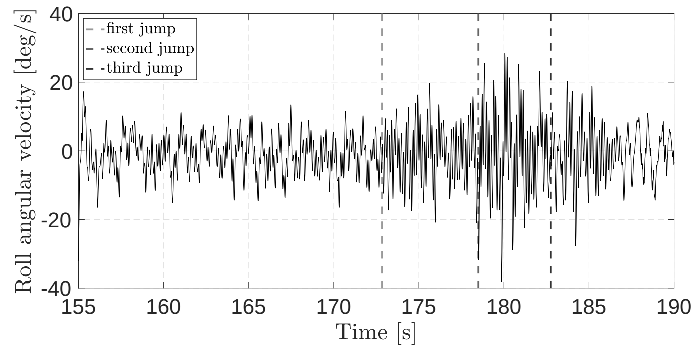

(b)

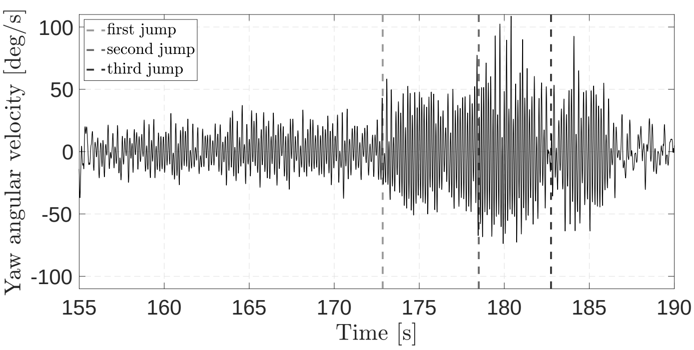

(c)

Figure 4. Data recorded during shimmy by IMU2 on the stem. (a) lateral acceleration, (b) roll angular velocity, and (c) yaw angular velocity.

by the videos recorded by the GoPro located on the rider's chest and the video camera on the car. Thus, there could be a dependency between oscillation amplitude and the rider's body posture. In particular, when his upper body moves downward and forward, shimmy amplitude increases. Overall, in the time plots there is no evidence of any kind of discontinuity when shimmy appears.

Figure 5 shows the spectrogram of IMU2 lateral acceleration. The frequency of wobble appears as a white horizontal line. In the beginning, shimmy frequency is about $f = 6.9$ Hz. When the first jump occurs, the oscillations frequency varies to $f = 7.2$ Hz. The same happens for the second and the third jumps ($f = 7.4$ Hz and $f = 7.1$ Hz respectively). After all, the frequency decreases as shimmy fades out. Although to a small

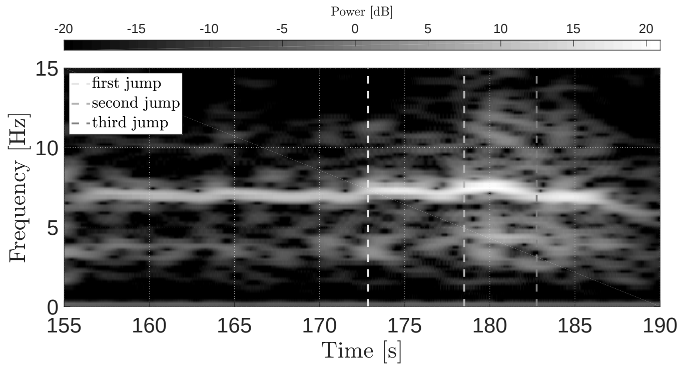

Figure 5. Spectrogram of IMU2 lateral acceleration recorded during shimmy.

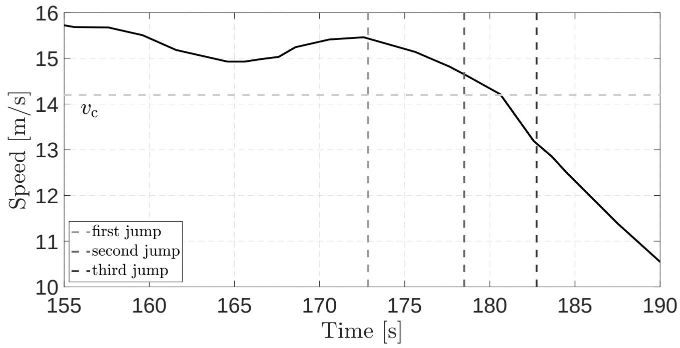

Figure 6. Bicycle forward speed in the shimmy time interval. The road becoming flat ensures the speed reduction.

extent, shimmy frequency seems to be coupled to its oscillation amplitude.

Figure 6 is a plot of the bicycle forward speed. From a comparison with Figure 5, wobble frequency and amplitude appear to be independent of speed. This confirms the results stated in [8], in which a mathematical model of bicycle-rider combination used in this on-road test is studied with methods of nonlinear dynamics. Bicycle geometrical properties, rider's posture and his anthropomorphic data are taken from [20].

Shimmy oscillations damp out at the end of the downhill when the forward speed decreases. The nonlinear analysis in [8] highlights that wobble should disappear when the speed is lower than a critical value equal to $v_c = 14.2$ m/s. Data collected in the experimental tests are in agreement with this numerical result, although there seems to be a delay in the disappearance of the oscillation. This hysteresis effect may be explained as a consequence of the forward deceleration of the bicycle while crossing the critical velocity v_c: it takes some time for the system to settle onto the stable equilibrium without shimmy oscillations. The same is true for wobble onset, i.e. forward acceleration has a stabilizing effect on oscillations and delays their onset at a forward speed $v > v_c$, except for the restart at about $t = 183$ s. That behavior is not explained by the model and might be due to a perturbation coming from the asphalt or the rider reinforcing previous oscillations, not completely damped. The hysteresis was also found in previous on-road tests in 2011 and 2014, as described in [8, 23]. Figure 7 shows the magnitude of IMU2 lateral acceleration maximum amplitude as a function of the forward speed, after being filtered with a band-pass filter with cut-off frequencies $f_{clow} = 4$ Hz and $f_{chigh} = 10$ Hz, so that, only wobble oscillations are taken into account. The starting time instant is indicated by a light grey pentagon on the right ($t = 135$ s), while the final time value is represented by a dark grey dot on the left ($t = 200$ s). This time interval

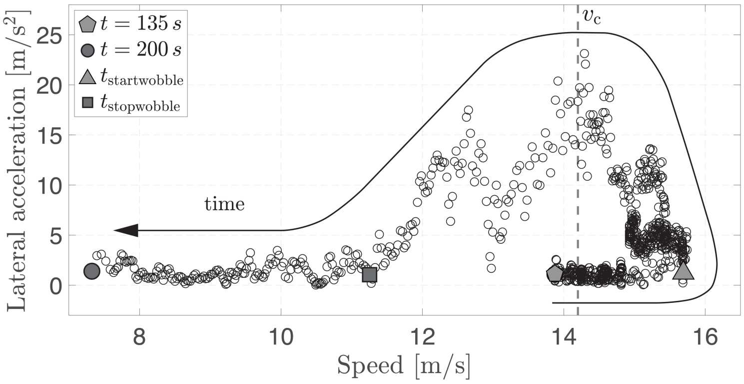

Figure 7. Magnitude of IMU2 lateral acceleration maximum amplitude as a function of the forward speed. The signal is filtered with a band-pass filter to consider only wobble oscillations. Time direction is indicated by the arrow, starting from the light grey pentagon on the bottom right. The hysteretic loop can be recognized near the critical speed v_{c}.

contains the entire shimmy phenomenon, as it occurs when $t > t_{\mathrm{startwobble}} = 155$ s and $t < t_{\mathrm{stopwobble}} = 190$ s. An arrow that moves counter-clockwise shows the direction of the test time. The hysteretic loop can be easily recognized both in the appearance and disappearance of wobble while crossing the threshold speed v_{c}.

4.1. *Rear Frame Motion*

Another important aspect of this analysis is to understand how the bicycle actually moves during shimmy. Thus, data recorded by the IMUs located on the rear frame are now compared. Lateral accelerations and roll and yaw angular velocities need to be considered jointly. To perform a direct comparison, all IMUs data need to be expressed in a single reference frame. As a consequence, the following bicycle coordinate system has been introduced as the reference frame for these IMUs (Figure 1, top-right):

- x_{r}-*axis* is in the symmetry plane of the vehicle and directed from the rear wheel to the front wheel (roll axis);
- z_{r}-*axis* is in the bicycle symmetry plane, normal to the roll axis and pointing towards the ground (yaw axis);
- y_{r}-*axis* completes a left-handed reference frame (pitch axis).

Figure 8 shows the lateral accelerations of the IMUs on the rear frame with respect to the bicycle reference system. In particular, the amplitude of these oscillations is larger near the front frame (IMU3), while it decreases moving towards the rear wheel (IMU6): the largest lateral displacement is near the head tube. The same can be observed moving from the bottom bracket to the saddle (IMU5 w.r.t. IMU4). The fundamental frequency of all signals in Figure 8 is the wobble frequency, and they have growing phase shift passing from IMU3 (head tube) to IMU6 (dropouts) since wobble is a vibrational mode that arises from the front frame.

Figure 9 shows the roll angular velocities recorded by the IMUs. As can be seen, all signals have two main harmonics: a low-frequency (1-2 Hz) one (weave mode), describing the rigid motion of the bicycle frame about the roll axis, and a higher frequency one, namely the wobble mode harmonics. The weave mode has the same amplitude and phase shift for all IMUs (not shown), while the wobble mode amplitude gets smaller and smaller passing from the steering assembly to the rear wheel hub. Figure 9 also shows the signals

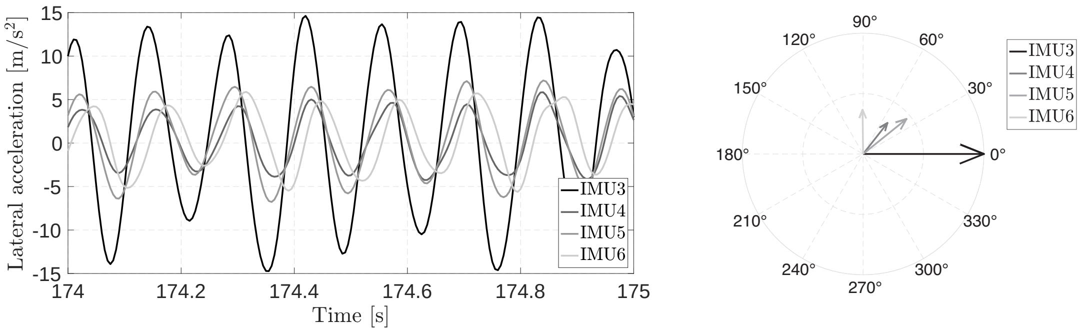

Figure 8. Lateral accelerations during shimmy recorded by IMUs on the rear frame and their phase diagram at $f = 7.2$ Hz.

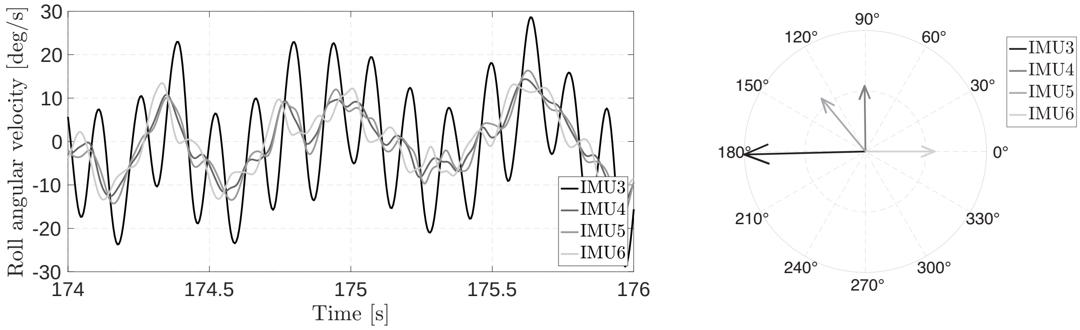

Figure 9. Roll angular velocities during shimmy recorded by IMUs on the rear frame and their phase diagram at $f = 7.2$ Hz.

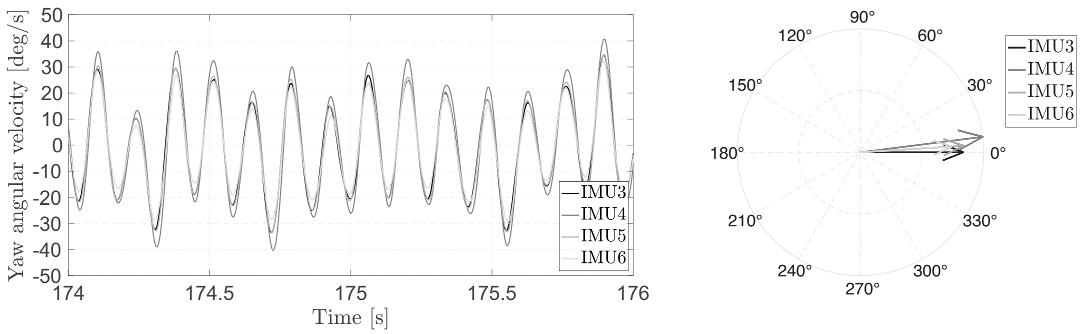

Figure 10. Yaw angular velocities during shimmy recorded by IMUs on the rear frame and their phase diagram at $f = 7.2$ Hz.

phase diagram at the wobble frequency: IMU3 and IMU6 are practically in anti-phase. This proves a relative torsion between the front triangle of the bicycle frame (IMU3) and its rear triangle (IMU4, IMU5 and IMU6).

Figure 10 illustrates the yaw angular velocities measured by the IMUs. The weave and wobble harmonics are still present. The fundamental result here is that also all the wobble harmonics have the same phase and amplitude, except for minor differences likely due to mechanical fixing inaccuracies or compliances. This shows that the bicycle frame moves (oscillates) almost rigidly around a vertical axis, at both weave and wobble frequencies.

The amplitude of the wobble is remarkable. Compared to Figure 9, Figure 10 shows that, unlike the weave mode amplitudes, the wobble mode amplitude of yaw angular velocities of the rear frame is greater than the amplitudes of roll angular velocities. This result is coherent with what is obtained in [9] by using a complex multi-body model of the racing bicycle.

Concerning the rigid oscillation of the bicycle frame, understanding where the angular velocity comes from is a crucial point to understand the shimmy onset and persistence. There are reasonably two main sources:

① the lateral oscillatory motion of the bicycle, as measured by the IMUs and seen from the videos;

② the overall compliance about a vertical axis of the rear frame, due to the possible compliance of the hub with respect to the plane of the wheel, of the wheel itself, and to the elastic deformation of the tyre.

Further laboratory and on-road trials are needed and planned to distinguish between these two contributions.

The rear frame compliance and the decreasing trend of lateral acceleration of the bicycle frame from IMU3 to IMU6 support the so-called ρ-axis compliant model [23, 24], which lumps the overall compliance about a vertical axis (the ρ-axis) located in the bicycle symmetry plane close to the rear wheel hub. According to [24], this compliance model can be used as an alternative to the more common β-axis torsional frame compliant model to predict the wobble mode [10, 11, 23, 25]. The above experimental results, with the reinforcement of those in Section 4.3, show that both these compliances are involved in the shimmy occurrence, although it is sufficient to include one of the two, taking on the overall compliance, to obtain a model of the bicycle capable of predicting the wobble mode.

The ρ-axis modelling idea is related to the shimmy problem of a simple trailing wheel system with yaw and lateral degrees of freedom, as described in [26].

Under the assumption that the bicycle frame is moving with rigid rotations about a vertical axis, based on the lateral accelerations in Figure 8, an estimated position of the vertical rotation axis can be computed. After filtering band-pass the IMUs signals to consider only shimmy oscillations, excluding some outliers in the processed data, and computing a mean value, the rotation axis turns out very close to the rear hub, as shown in Figure 1.

4.2. *Front Frame Motion*

In this Section, the behaviour of the front assembly is studied. By comparing data records of IMU1 and IMU2, a new coordinate system is chosen as reference frame (see Figure 1, top-left):

- z_f*-axis* in the symmetry plane of the front assembly, directed as the head tube and pointing to the ground (steering axis);
- x_f*-axis* in the symmetry plane of the front assembly and normal to z_f*-axis*, pointing the forward direction. This axis is parallel to the β-axis introduced above (see Figure 1);
- y_f*-axis* completes a left-handed reference frame.

As can be seen in Figure 11, the front assembly made up of fork and handlebar rigidly rotates about the steering axis. This is due to the degree of freedom allowed by the ball bearings in the head tube. Indeed, there is no relative torsion between IMU1 and IMU2 during shimmy, so the front frame can be considered as a rigid body along this direction.

This is no longer true if angular velocities about front frame x_f*-axis* are considered.

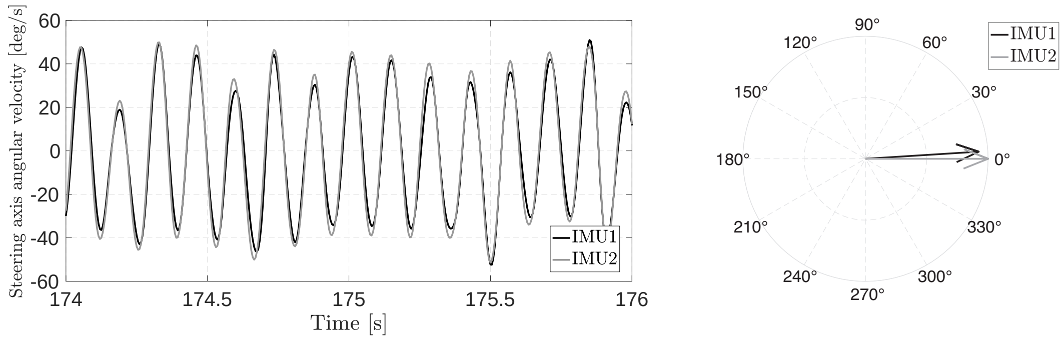

Figure 11. Angular velocities of the front frame about the steering axis during shimmy and their phase diagram at $f = 7.2$ Hz.

Referring to Figure 12(a), both signals have the same low-frequency behaviour, representing a rigid motion about this axis. This has been proved by using a low-pass filter with a cut-off frequency $f_\mathrm{c} = 5$ Hz (not shown). However, there is also a relative motion at the wobble frequency between the two extreme points of the front assembly. To better understand this behaviour, IMU1 and IMU2 roll angular velocities are now filtered with a band-pass filter with $f_\mathrm{clow} = 4$ Hz and $f_\mathrm{chigh} = 10$ Hz. As can be seen in the phase diagram in Figure 12(b), at the wobble frequency the two signals have almost the same amplitude but they are in anti-phase. While it is expected that the fork undergoes a lateral bending (in the direction of y_f-*axis*), forced by the headset, likely a rigid body (see Section 4.3 for the roll angular velocity measured by IMU3 close to the head tube), understanding the roll angular velocity measured by IMU2 is more challenging, and will probably require further experiments and numerical analysis. In fact, the stem rotates about the head tube axis, which is subjected to a roll angular velocity as measured by IMU3, but IMU2 roll angular velocity is quite different from that of the head tube (see next Section). Supposedly, the roll angular velocity measured by IMU2 better represents the torsion of the stem in the x_f-*axis* direction, rather than the lateral bending deformation of the upper part of the fork. A possible contribution to the stem angular velocity may derive from inertia torque generated by the masses of the rider's forearms and hands, firmly attached to the lower part of the handlebar which is rotating about the steering axis and subjected to strong lateral accelerations.

The analysis of IMU1 linear accelerations give further insights, not just about the fork motion. Figure 13 shows the longitudinal acceleration as a function of the lateral acceleration in a shimmy interval of one second. Both accelerations are band-pass filtered to extract only the wobble components. The graph shows a cyclical behavior, as predicted by the nonlinear analysis in [8], and shows a lateral and longitudinal oscillatory motion at the height of the front hub, but likely also of the front road-tyre contact point. Accelerations, about a quarter of the cycle out of phase each other, require road-tyre contact forces with the same phase shift, which reasonably have a major role in the shimmy mechanism.

According to [27], the lateral displacement of the fork, together with its rotation about the steering axis, modifies the orientation of the front wheel with respect to the road surface and can alter the geometry of the entire steering system. As a consequence, the front wheel starts to move following an oscillatory motion, and the resulting forces at the front contact point can produce a positive steering feedback that causes the self-excitation of wobble. Fortunately, as stated in [8], shimmy is a stable limit cycle, which means that oscillations have limited amplitude and they do not diverge causing the fall of the rider (confirmed by Figure 13).

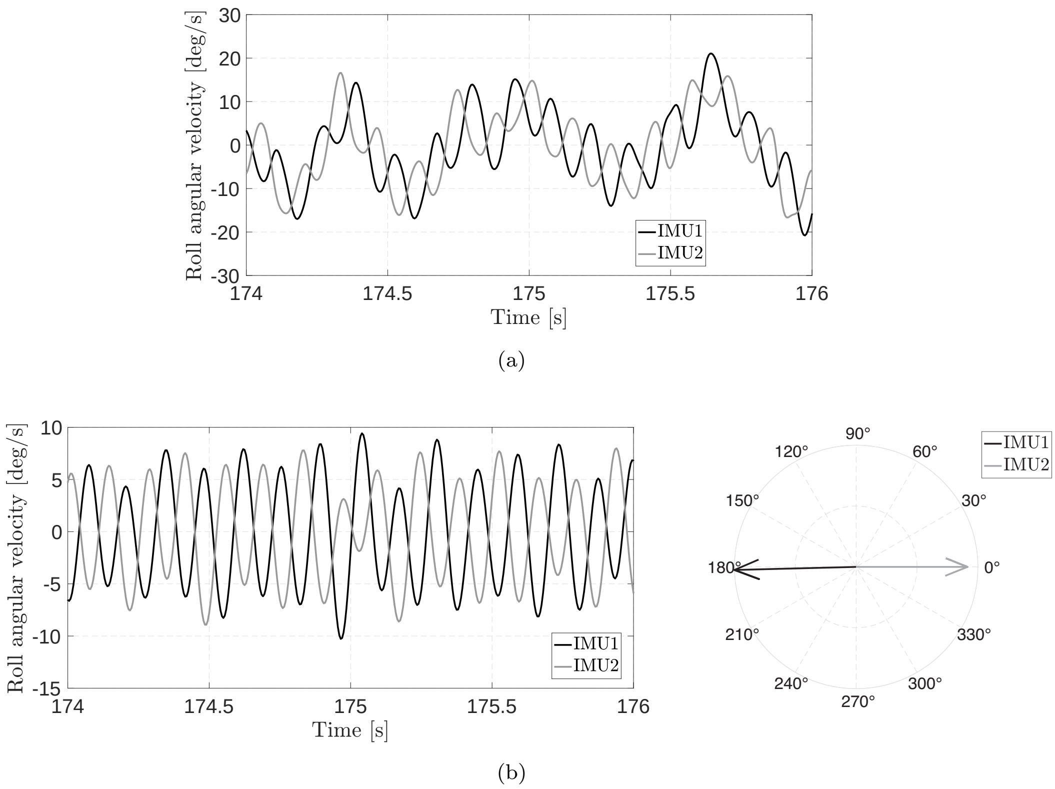

Figure 12. Angular velocities of the front frame about the roll axis during shimmy. (a) without filter and (b) with a band-pass filter to consider only wobble oscillations. The phase diagram is shown at $f = 7.2$ Hz.

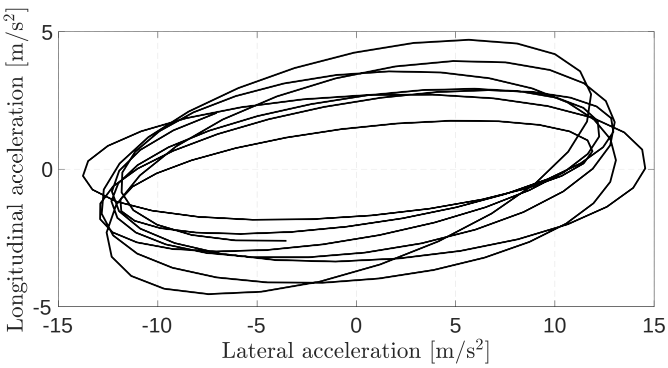

Figure 13. Accelerations recorded by IMU1 on the front hub: longitudinal acceleration as a function of the lateral acceleration. Signals are band-pass filtered to consider only wobble oscillations during 1 second.

4.3. *Front and Rear Frames Motion*

In previous Sections, the movement of the two bicycle main parts has been studied separately. Here, the relative motion between front and rear frames is examined. Data recorded by IMU1, IMU2, and IMU3 are analyzed after being expressed in the bicycle reference frame $x_\mathrm{r}y_\mathrm{r}z_\mathrm{r}$ (introduced in Section 4.1) and band-pass filtered to highlight only wobble oscillations. Figure 14 shows their roll angular velocities with their phase diagram. As can be seen, IMU1 and IMU3 are almost in phase, while IMU2 is in anti-phase with respect to the others. Thus, the torsion of the bicycle frame about the roll axis x_r (IMU3) has the same rotation-wise of the front frame lower part lateral bending (IMU1). The stem rotates instead in the opposite direction (IMU2). Moreover, the amplitude of the

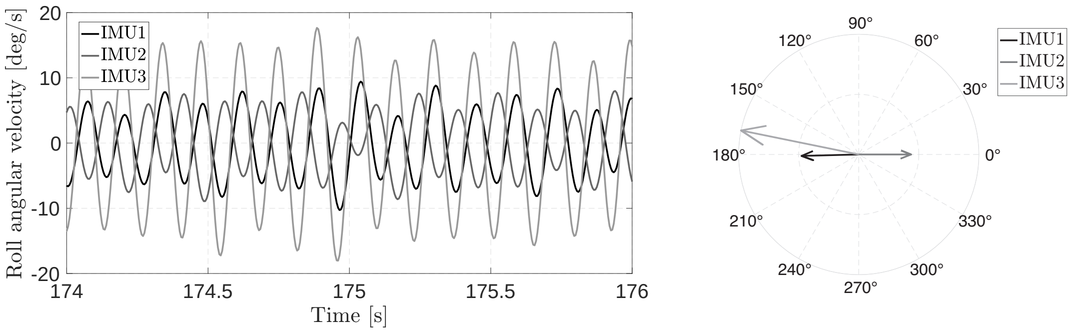

Figure 14. Roll angular velocities during shimmy recorded by IMUs on front and rear frames with a band-pass filter to consider only wobble oscillations. The phase diagram is shown at $f = 7.2$ Hz.

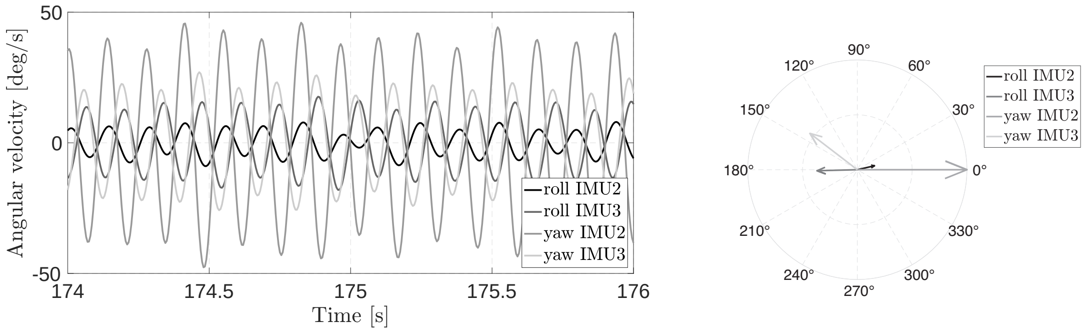

Figure 15. Roll and yaw angular velocities during shimmy recorded by IMUs on front and rear frames with a band-pass filter to consider only wobble oscillations. The phase diagram is shown at $f = 7.2$ Hz.

top tube (IMU3) roll angular velocity is almost double compared to that of the fork close to the front hub (IMU1). As already mentioned, further studies are needed to explain the stem angular velocity (IMU2), about half in amplitude compared to that of the IMU3 but of opposite sign.

Figure 15 shows roll and yaw angular velocities recorded by IMU2 and IMU3 with their phase diagram. IMU2 roll angular velocity is almost in phase with its yaw angular velocity, while it is in anti-phase with respect to the roll angular velocity of the rear frame (IMU3). On the other hand, IMU3 yaw angular velocity is out of phase compared to that of the front assembly (IMU2). Furthermore, oscillations about the steering axis (yaw IMU2) are larger than rear frame yaw rotations measured by IMU3.

Considering all the results found up to this point, a complete description of the complex bicycle motion during shimmy can be provided. As confirmed by data (e.g., Figure 13) and videos recorded during the on-road test activity, the front wheel-road contact point describes an oscillatory path along the average forward motion direction. The amplitude of these oscillations depends on four main contributions:

① the torsion of the bicycle frame along the longitudinal direction (x_r-axis);
② the lateral bending deformation of the fork along the y_f-axis (see Figure 4.3(left));
③ the tyre lateral deformation due to their elastic properties;
④ the overall compliance of the rear frame about a vertical axis, located near the rear hub and the rear wheel.

Figure 4.3(left) also shows the relative, opposite, roll motion of the handlebar with respect to lower part of the fork, while Figure 4.3(right) sketches a top view of bicycle motion: the front frame rotates counter-clockwise about the steering axis, whereas the bicycle

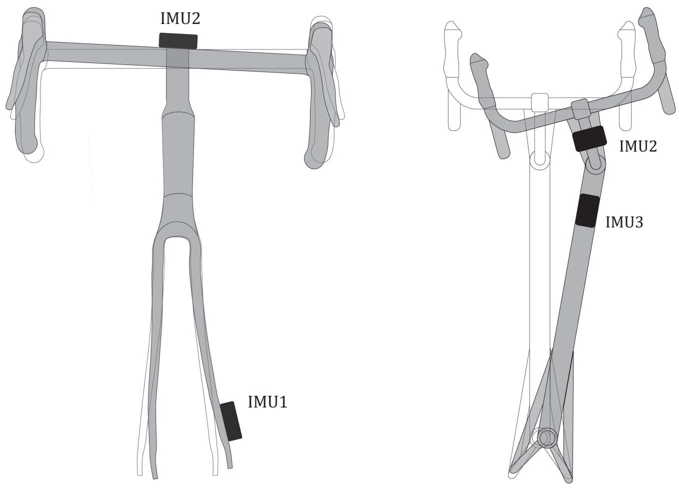

Figure 16. Front and rear frames deformation during shimmy. Deformations are exaggerated to better understand the motion; (left) front view and (right) top view.

frame rotates (rigidly) clockwise about a vertical axis close to the rear wheel hub. The same happens in the opposite direction when the front assembly is steered to the right, until the forward speed decreases at the end of the descent.

5. Discussion

This paper provides original records of forward speed, linear accelerations, and angular velocities gathered in six selected points of a professional carbon fiber racing bicycle undergoing a strong shimmy. The shimmy onsets spontaneously during a medium slope downhill, while riding at high speed (over 14 m/s), with hands firmly on the handlebar and without pedalling. All data were collected by a stand-alone acquisition system able to sample three acceleration and three angular velocity synchronous measures of the six selected points on front and rear frames at 200 Hz sampling frequency, suitable to reconstruct correctly the about 7 Hz shimmy vibration.

All signals were low-pass filtered ($f_c = 20$ Hz) to remove high-frequency noise. Then, another low-pass filter with $f_c = 5$ Hz was used to assess the rigid-body behaviour (i.e., the weave mode) of the bicycle, and a band-pass filter ($f_{clow} = 4$ Hz and $f_{chigh} = 10$ Hz) to highlight the behaviour of the front and rear frames at the wobble (shimmy) frequency. Their analysis shows that both frames act rigidly below 5 Hz, while at the shimmy frequency they undergo additional relative motions and deflections. For instance, the bicycle frame oscillates rigidly about a vertical axis, while in the longitudinal direction (roll) it is subjected to a relative torsion between the head tube and the rear dropouts. To some extent, the same behaviour can be associated to the front frame, which undergoes a rigid motion about the steering axis in the whole frequency range, due to the degree of freedom provided by the steering assembly, while it is subjected to a bending in the y_f-*axis* direction at the shimmy frequency.

Overall, the trends of the linear accelerations and angular velocities recorded by the six IMUs appear to be intrinsically coherent with each other and also with what is perceived by the rider and detectable by videos, as well as they help to better understand the shimmy mechanism.

6. Conclusion

All the above results show that the overall bicycle motion during shimmy is complex, characterized by violent oscillations of the front frame but also involving the rear frame, to a decreasing extent from the head tube to the dropouts. The observed motion of the vehicle validates the introduction in mathematical models to study shimmy of both the two additional degrees of freedom proposed in the literature:

- ρ-axis, laying close to the rear wheel hub and lumping the overall compliance of the rear part of the bicycle about a vertical axis. This compliance allows the bicycle frame to oscillate rigidly;
- β-axis, laying in the rear frame plane, normal to the head tube, representing the fork lateral bending and the torsional compliance of the bicycle frame with respect to the longitudinal (roll) direction. This compliance is lumped near the stem.

Jointly ρ and β axes describe the overall compliance and lateral motions of the bicycle. Their knowledge can give bike designers the right hints to devise (more) shimmy free bicycles and will be the subject of further research, in particular to clarify the compliance contribution of any component of the bicycle.

The analysis of acceleration records confirmed that the shimmy frequency is independent of the bicycle forward speed, and it is only slightly dependent on the oscillation amplitude. Comparing acceleration records and action cam images highlighted that a change in the rider's body position may cause variation of shimmy oscillation amplitude but not its frequency. Comparing acceleration and forward speed records has confirmed the hysteretic behaviour of shimmy with respect to forward speed, namely that the shimmy onset speed is much higher than the fade out one. In [8] it is conjectured that the vehicle acceleration while crossing the critical velocity (the shimmy onset theoretical velocity) causes a delay (in the sense of higher speed) in the appearance of shimmy. The same happens in the opposite direction: it takes some time for the system to settle onto the no-shimmy stable equilibrium while decelerating.

This is very important for a rider who is facing shimmy: he or she has to try not to fall, and not to hit other vehicles or go off-road, for the time necessary to decrease the speed below the threshold of the disappearance of shimmy. Unfortunately, this is a rather difficult task if the road remains very sloping and curvy because brakes cannot be used effectively when cornering, and they may, at first, cause an increase in the amplitude of the steering oscillation.

References

[1] Bozak D. Wintergreen cycling camp speed wobble. 2011 Mar; Available from: https://www.youtube.com/watch?v=VfngbsIUSj8.
[2] Petraitis A. Road bike high speed wobble 1st person view (shimmy). 2014 Jun; Available from: https://www.youtube.com/watch?v=hMNFS2ap3fU.
[3] Brandt J. Shimmy or speed wobble. 2004 Jun; Available from: http://www.sheldonbrown.com/brandt/shimmy.html.
[4] Brett M. How to cure speed wobbles. 2018 Aug; Available from: https://road.cc/content/feature/219888-how-cure-speed-wobbles.
[5] Rinard D. Bicycle shimmy or speed wobble. 2007 Sep; Available from: https://www.youtube.com/watch?v=xODNzyUbIHo.
[6] Empfield D. Speed wobble. 2015 Apr; Available from: http://www.slowtwitch.com/Tech/SpeedWobble5033.html.

[7] Meijaard J, Papadopoulos JM, Ruina A, Schwab A. Linearized dynamics equations for the balance and steer of a bicycle: a benchmark and review. Proceedings of the Royal Society of London A: Mathematical, Physical and Engineering Sciences. 2007;463(2084):1955–1982; Available from: http://rspa.royalsocietypublishing.org/content/463/2084/1955.

[8] Tomiati N, Colombo A, Magnani G. A nonlinear model of bicycle shimmy. Vehicle System Dynamics. 2018;0(0):1–21; Available from: https://doi.org/10.1080/00423114.2018.1465574.

[9] Tomiati N, Magnani G, Scaglioni B, Ferretti G. Model based analysis of shimmy in a racing bicycle. In: Proceedings of the 12th International Modelica Conference; 2017 May 15–17; Prague, Czech Republic; 2017. p. 441–447.

[10] Limebeer DJN, Sharp RS. Bicycles, motorcycles and models. IEEE Control Systems Magazine. 2006 October;26:34–61.

[11] Plöchl M, Edelmann J, Angrosch B, Ott C. On the wobble mode of a bicycle. Vehicle System Dynamics. 2012;50(3):415–429; Available from: http://dx.doi.org/10.1080/00423114.2011.594164.

[12] Cossalter V, Doria A, Lot R, Massaro M. The effect of rider's passive steering impedance onmotorcycle stability: identification and analysis. Meccanica. 2011 Apr;46(2):279–292; Available from: https://doi.org/10.1007/s11012-010-9304-1.

[13] Pacejka HB. Analysis of the shimmy phenomenon. Proceedings of the Institution of Mechanical Engineers: Automobile Division. 1965;180(1):251–268.

[14] Raspberry pi foundation. 2018; Available from: https://www.raspberrypi.org/.

[15] Arduino 101. 2018; Available from: https://store.arduino.cc/genuino-101.

[16] Intel curie module. 2018; Available from: https://www.intel.com/content/dam/support/us/en/documents/boardsandkits/curie/intel-curie-module-datasheet.pdf.

[17] Bosch bmi 160 inertial measurement unit. 2018; Available from: https://ae-bst.resource.bosch.com/media/_tech/media/datasheets/BST-BMI160-DS000-07.pdf.

[18] Henderson G. Wiring pi library for raspberry pi. 2018; Available from: http://wiringpi.com/.

[19] MathWorks. Matlab. 2018; Available from: https://www.mathworks.com/products/matlab.html.

[20] Klinger F, Nusime J, Edelmann J, Plöchl M. Wobble of a racing bicycle with a rider hands on and hands off the handlebar. Vehicle System Dynamics. 2014;52(sup1):51–68; Available from: http://dx.doi.org/10.1080/00423114.2013.877592.

[21] Garmin. Edge 820. 2018; Available from: http://static.garmin.com/pumac/Edge_820_OM_EN.pdf.

[22] GoPro. Hero3+. 2018; Available from: https://it.gopro.com/content/dam/help/hero3plus-silver-edition/manuals/UM_H3PlusSilver_ENG_REVB_WEB.pdf.

[23] Magnani G, Papadopoulos J, Ceriani NM. On-road measurements of high speed bicycle shimmy, and comparison to structural resonance. In: Proceedings of the IEEE International Conference on Mechatronics; 2013; Vicenza, IT; 2013. p. 400–405.

[24] Nusime J, Klinger F, Edelmann J, Magnani G, Plöchl M. Some considerations on modelling bicycle wobble at high speed. In: Proceedings of Bicycle and Motorcycle Dynamics; 2013 November 11–13; Narashino, Japan; 2013.

[25] Doria A, Favaron V, Roa S. A doe approach for evaluating the effect of bicycle properties on stability. In: Proceedings of the ASME 2017 International Design Engineering Technical Conferences and Computers and Information in Engineering Conference; 2017 August 6–9; Cleveland, Ohio, USA; 2017.

[26] Pacejka HB. Tire and vehicle dynamics. 3rd ed. Oxford: Butterworth-Heinemann; 2012.

[27] Cossalter V. Motorcycle dynamics. 2nd ed. www.lulu.com; 2006.